Journal of Power Sources 279 (2015) 55–63

Contents lists available at ScienceDirect

Journal of Power Sources

journal homepage: www.elsevier.com/locate/jpowsour

Simulation of ionomer membrane fatigue under mechanical and hygrothermal loading conditions

Ramin M.H. Khorasany, Erik Kjeang*, G.G. Wang, R.K.N.D. Rajapakse

School of Mechatronic Systems Engineering, Simon Fraser University, 250-13450 102 Avenue, Surrey, BC V3T 0A3, Canada

HIGHLIGHTS

- A numerical membrane fatigue model based on the finite element method is proposed.
- The fatigue lifetime is found to be shorter at points under strain concentrations.
- The fatigue lifetime is shorter under humidity cycling than temperature cycling.
- The effect of strain amplitude is more substantial than for mean strain.
- Simultaneous cycling of RH and T substantially decreases the fatigue lifetime.

GRAPHICAL ABSTRACT

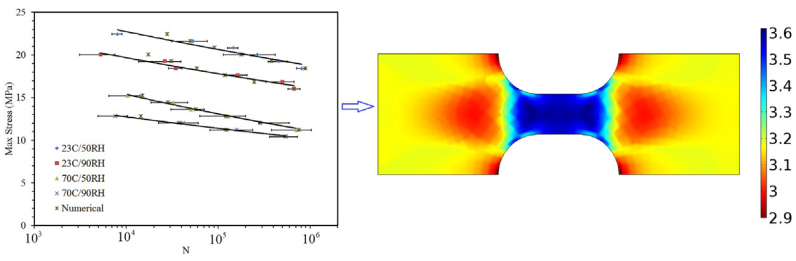

ARTICLE INFO

Article history:
Received 21 October 2014
Accepted 26 December 2014
Available online 27 December 2014

Keywords:
Fuel cell
Membrane
Fatigue model
Finite element
Durability

ABSTRACT

Understanding the fatigue lifetime of common perfluorosulfonic acid (PFSA) ionomer membranes under fluctuating hygrothermal conditions is essential for the development of durable fuel cell technologies. For this purpose, a finite element based fatigue lifetime prediction model is developed based on an elastic–plastic constitutive model combined with a Smith-Watson-Topper (SWT) fatigue formulation. The model is validated against previously reported experimental results for a membrane under cyclic mechanical loadings. The validated model is then utilized to investigate the membrane fatigue lifetime in ex-situ applications under cyclic humidity and temperature conditions. The simulations suggest that the membrane fatigue lifetime is shorter under fluctuating humidity loadings than for temperature loadings. Additionally, the membrane fatigue lifetime is found to be more sensitive to the amplitude of the strain oscillations than to the mean strain under hygrothermal cycling. Most notably, the model predicts that simultaneous humidity and temperature cycling can exacerbate the fatigue process and reduce the fatigue lifetime by several orders of magnitude compared to isolated humidity or temperature cycling. The combination of measured mechanical fatigue data and the present numerical model provides a useful toolkit for analysis of membrane fatigue due to hygrothermal variations, which can be costly and time-consuming when addressed experimentally.

1. Introduction

The Polymer Electrolyte Fuel Cell (PEFC) is a promising technology for providing clean energy for a wide range of applications from automotive to portable and stationary power generation [1].

* Corresponding author.
E-mail address: ekjeang@sfu.ca (E. Kjeang).

http://dx.doi.org/10.1016/j.jpowsour.2014.12.133
0378-7753/

The Membrane Electrolyte Assembly (MEA) inside each fuel cell consists of a polymer electrolyte membrane and an electrode on either side. The overall lifetime of the fuel cell stack is primarily restricted by MEA durability and more specifically by membrane and catalyst layer degradation, where hydrogen leaks due to membrane damage is usually the main lifetime-limiting factor [1]. Reliable fuel cell operation requires the membrane to have good ionic conduction while separating the hydrogen on the anode from the oxygen on the cathode. Commonly used perfluorosulfonic acid (PFSA) ionomer membranes rely on water sorption to facilitate the desired functionality and are therefore sensitive to external conditions. Stringent requirements for performance and cost have recently led to the use of thinner membranes, which in turn has imposed durability issues. According to the United States Department of Energy, the target durability of the fuel cell stack is 5000 h for cars and 40,000 h for stationary applications [2], which poses a considerable challenge for fuel cell developers and warrants further research towards a deeper understanding of the fundamental degradation mechanisms.

The degradations mechanisms in PFSA ionomer membranes can be divided into two main categories: mechanical and chemical degradation mechanisms [3,4]. Chemical membrane degradation is caused by the reaction of radicals such as hydroxyl and hydroperoxyl radicals with chemical bonds in the ionomer structure [5–9]. Radicals have been shown to attack carboxylic acid end group sites of the main chain and sulfonic acid groups in the side chain [7,8]. Chemical membrane degradation results in general thinning and creation of pinholes and divots [10].

Mechanical membrane degradation is believed to be caused by the excessive expansion and contraction of the membrane generated via water sorption and desorption during variations in local hygrothermal conditions [11]. Inside the fuel cell, the membrane is confined by the adjacent MEA components and compressed between the bipolar plates [12]. Due to such confinements, variations in water sorption and associated strain lead to fluctuating mechanical stresses in the membrane [13]. With repeated stress cycles, microcracks will eventually initiate and propagate towards mechanical failure [14]. The mechanical behavior of the membrane is intricately linked to its mechanical properties, which have been measured experimentally for both membranes [10,12,15,16] and catalyst coated membranes [17] under various types of hygrothermal and mechanical loadings. Experimental results for PFSA ionomer membranes generally exhibit a linear response governed by fundamental elasticity theories [18,19] for strain below the yield point followed by a nonlinear phase associated with plastic deformation [20]. It is further established that the mechanical characteristics of the membrane are time, temperature, and humidity dependent [21]. Provided that mechanical degradation depends on cyclic stresses and strains, accurate knowledge of the stress and strain profiles in the membrane is essential [12,14,21–24]. Constitutive relations that correlate stress to induced strain have been developed [13,18,22,23,25–27] and utilized to simulate the in-situ response of the membrane to external hygrothermal loadings [11,28,29].

Fatigue is the internal process that occurs when a material is subjected to cyclic stress, whereby bonds between inner elements gradually deteriorate and permanent, localized structural damage starts to appear. Having important implications in a wide range of industry sectors, the mechanical fatigue phenomena have been systematically studied for common types of materials such as metals [30]. The key parameter that defines the material lifetime in the fatigue process is the severity of the load variations [31]. In the case of a fuel cell membrane, in-situ simulations have predicted internal stress fluctuations from compressive to tensile forces under hygrothermal cycling [11,28]. Notably, these stress fluctuations are also associated with dramatic tensile and compressive plastic strains [11]. Temporal, recurrent changes in stress and strain during regular duty cycle operation therefore makes the membrane susceptible to crack initiation due to material fatigue followed by crack propagation and fracture [32–36].

Recognizing that mechanical membrane degradation and associated failures are an important factor for the overall fuel cell durability, several studies have been conducted to characterize its behavior [4,22]. The most commonly employed test is the US Department of Energy endorsed standardized accelerated stress test for mechanical membrane degradation, which is conducted by subjecting an MEA to in-situ humidity cycles. In these tests, the rate of gas crossover is measured as an indication of the level of mechanical damage in the membrane, while the test is continued up to 20,000 cycles [2,37]. Given the relatively large number of cycles, material fatigue is expected to play a significant role in the degradation process. Alternatively, material fatigue tests can be conducted ex-situ by subjecting membrane specimens to mechanical cyclic loadings under controlled environmental conditions [13,38]. Recent ex-situ experiments have shown that the membrane fatigue lifetime decreases exponentially with increasing applied stress [38].

A main challenge in membrane fatigue analysis lies in the development of numerical tools capable of predicting fatigue lifetime under cyclic mechanical and hygrothermal loadings. Most previous work on fatigue has been experimental, and there is a lack of fundamental based modeling tools in this area. Moreover, due to the complexity of fatigue modeling, the existing numerical investigations were based upon empirical relations [14,38]. The main objective of the present work is therefore to develop a finite element based fatigue model that is capable of predicting the membrane lifetime and lifetime distribution under a simulated fatigue test. Numerical finite element simulations are used to find the amplitude of the fluctuating strain at the environmental conditions investigated in our previously published fatigue experiments [13]. The Smith-Watson-Topper (SWT) approach is utilized to develop a numerical model for predicting the ex-situ fatigue response of the membrane. The developed numerical scheme is then used to investigate the effect of mechanical and hygrothermal cyclic loadings on the membrane lifetime. The proposed model is intended to enhance the fundamental understanding of the fatigue process and corresponding mechanical durability of the membrane under conditions that are relevant for fuel cell operation.

2. Model description

As previously mentioned, fatigue based mechanical membrane degradation is caused by cyclic hygrothermal and mechanical loads applied during fuel cell operation. In addition to the amplitude of stress and strain fluctuations, the mean values of the oscillations can also affect the mechanical fatigue process. Therefore, a comprehensive fatigue model that captures the effects of both hygrothermal and mechanical variations and pre-existing conditions is sought. The model is intended to take the stress and strain conditions as input, which can be facilitated by an embedded finite element model, and predict the membrane fatigue lifetime distribution as output. The proposed membrane fatigue modeling framework therefore consists of two main sub-models: a constitutive relation for the stress-strain behavior of the membrane; and a fatigue algorithm that can identify the crack initiation threshold and lifetime distribution.

2.1. Constitutive relation

Our previously published tensile experimental results suggest

that the stress-strain response of PFSA membranes consists of an elastic portion followed by a nonlinear plastic portion [17]. The modulus of elasticity and proportional strain limit was found to be a function of environmental conditions. Depending on the amplitude of the loading and environmental conditions, the membrane may experience elastic stresses and strains due to thermal expansion and hydration swelling. If the stress is beyond the yield stress, plastic strains are inevitable, which can be modeled using nonlinear plasticity constitutive relations with strain hardening. Hence, the total strain can be written as

$$\varepsilon_{ij} = \varepsilon_{ij}^{M} + \varepsilon_{ij}^{S} + \varepsilon_{ij}^{T} \tag{1}$$

where ε_{ij}^{M}, ε_{ij}^{S}, and ε_{ij}^{T} are the strain contributions due to mechanical loadings, hydration swelling, and thermal expansion, respectively. The contribution of the strain due to mechanical loadings can be decomposed to plastic (ε_{ij}^{p}) and elastic (ε_{ij}^{e}) strains as follows

$$\varepsilon_{ij}^{M} = \varepsilon_{ij}^{e} + \varepsilon_{ij}^{p} \tag{2}$$

where α^{T} is the thermal expansion coefficient. Thermal strain due to the difference between the current temperature (T) and the reference temperature (T_0), is assumed to be

$$\varepsilon_{ij}^{T} = \alpha^{T}(T - T_0)\delta_{ij} \tag{3}$$

where δ_{ij} is the Kronecker delta. Similarly for the swelling strain the following relation can be deduced [18].

$$\varepsilon_{ij}^{S} = \alpha^{RH}(RH - RH_0)\delta_{ij} \tag{4}$$

where α^{RH} is the hydration induced expansion coefficient for swelling, RH is the current value of relative humidity, and RH_0 is the reference value of relative humidity. The thermal expansion and swelling coefficients may depend upon environmental conditions and the plastic deformations, however the assumption of linear and isotropic coefficients is expected to be valid in this case [21,39].

For strains below the yield point, the linear relation between stress and strain is described by Hooke's law

$$\sigma_{ij} = \frac{E}{(1+\nu)(1-2\nu)}\left[\nu\varepsilon_{kk}^{e} + (1-2\nu)\varepsilon_{ij}^{e}\right] \tag{5}$$

where σ_{ij} represents the components of true stress, E is Young's modulus, ν is Poisson's ratio, and $\varepsilon_{kk}^{e} = \varepsilon_{11}^{e} + \varepsilon_{22}^{e} + \varepsilon_{33}^{e}$. At each environmental condition, the Young's modulus and Poisson's ratio are obtained from our previously reported data [17], and hence the numerical results will be valid for the range of loading conditions considered in the measurements. The incompressible nonlinear post yield response of the membrane is characterized using plastic flow according to the von Mises yield function [21,22,40].

$$f(\sigma_{ij}) = \sqrt{\frac{3}{2}S_{ij}S_{ij}} - \sigma_y \tag{6}$$

where σ_y is the yield stress and S_{ij} represents the components of the deviatoric stress (defined as $S_{ij} = \sigma_{ij} - 1/3\sigma_{kk}\delta_{ij}$ and $\sigma_{kk} = \sigma_{11}+\sigma_{22}+\sigma_{33}$). Experimental investigations have also revealed isotropic strain hardening [18]. Therefore, the yield stress depends upon the environmental conditions and the level of plastic strain as per

$$\sigma_y = \sigma_y(\varepsilon^{p}, T, RH) \tag{7}$$

where ε^{p} is the current equivalent plastic strain defined by

$$\varepsilon^{p} = \int \sqrt{\frac{2}{3}d\varepsilon_{ij}^{p}d\varepsilon_{ij}^{p}} \tag{8}$$

According to this model, yield occurs when the yield function is $f = 0$. The material exhibits plastic behavior when $f > 0$ and deforms elastically when $f < 0$.

2.2. Fatigue model

Fatigue modeling of other types of commonly used materials has been widely investigated in the literature [30,31]. However, to our knowledge, no prior studies have considered ionomer membranes. Two types of fatigue modeling approaches can be taken: stress based models; and strain based models. Stress based models are generally used to explore whether under a given state of loading a material can endure a certain number of cycles (e.g., one million cycles) without mechanical failure. In contrast, strain based models can be used to estimate the number of cycles for a given cyclic loading condition that a material can withstand before it fails due to fatigue fracture. The strain based approach is therefore more suitable in this case, given the objective to predict fatigue lifetime. Strain based models are generally developed based on the assumption that the fatigue life of the material is correlated to the level of oscillatory strain the material experiences. Cofin and Manson suggested that on a log–log scale there is a linear relationship between the fatigue lifetime and the amplitude of plastic oscillatory strain [41]. The Manson–Cofin relation is expressed by Ref. [42].

$$\frac{\Delta\varepsilon^{p}}{2} = \varepsilon_f'\left(2N_f\right)^{c} \tag{9}$$

where $\Delta\varepsilon^{p}/2$ is the amplitude of the plastic strain, ε_f' is the fatigue ductility coefficient, c is the fatigue ductility exponent, and N_f is the fatigue lifetime. A similar log–log relation is used to define the relationship between the amplitude of the oscillatory elastic strain and the fatigue lifetime [41–43].

$$\frac{\Delta\varepsilon^{e}}{2} = \frac{\sigma_f'}{E}\left(2N_f\right)^{b} \tag{10}$$

where $\Delta\varepsilon^{e}/2$ is the amplitude of the elastic strain, σ_f' is the fatigue strength coefficient, and b is the fatigue strength exponent. The total strain amplitude is the summation of the plastic and elastic strains. Hence, the fatigue model is obtained by

$$\frac{\Delta\varepsilon}{2} = \frac{\sigma_f'}{E}\left(2N_f\right)^{b} + \varepsilon_f'\left(2N_f\right)^{c}$$
$$\Delta\varepsilon = \Delta\varepsilon^{e} + \Delta\varepsilon^{p} \tag{11}$$

However, the above model does not yet account for the effect of mean stress. Hence, the Smith-Watson-Topper (SWT) equation is obtained by multiplying Eq. (11) by the maximum stress (σ_{max}, which is the summation of the mean stress and the amplitude of the fluctuating stress) according to

$$\sigma_{\max}\frac{\Delta\varepsilon}{2} = \frac{\left(\sigma_f'\right)^{2}}{E}\left(2N_f\right)^{2b} + \sigma_f'\varepsilon_f'\left(2N_f\right)^{b+c} \tag{12}$$

In the SWT model, a critical plane normal to the direction with the maximum strain range is considered. The membrane fatigue lifetime under hygrothermal and mechanical loadings is simulated by solving Eq. (12) based on the underlying constitutive relation using finite element analysis carried out in COMSOL Multiphysics version 4.3.

3. Results and discussion

In this section, the developed finite element based fatigue model is first validated against our previously published experimental fatigue data for PFSA membranes (Nafion® NR-211) subjected to cyclic mechanical loadings [13]. The material constants for the constitutive relations are based on those reported in our previous work [17]. For the fatigue simulations, the material properties are obtained on the experimental results in Ref. [13] and summarized in Table 1. The validated model is then used to study the effect of cyclic temperature and relative humidity conditions on the fatigue lifetime of the membrane. Additionally, the influence of a pre-existing stress on the membrane lifetime is investigated.

3.1. Model validation

The validity of the numerical model is first investigated by simulating the action of the fatigue experiments described in our previous work [13]. In order to avoid stress concentration effects at the edges, specimens for fatigue testing were prepared in dogbone shapes [38], as shown in Fig. 1. Provided the high aspect ratio of the thin-film membrane specimens, a plane stress distribution is assumed. The tensile fatigue experiment is simulated by applying a clamped boundary condition for the left edge and a free boundary condition for all other boundaries (cf., Fig. 1a) while a mechanical load comprising of a mean force combined with an oscillatory force is applied to the right edge as a distributed load. The ratio of the minimum force to maximum force is chosen to be 0.2, in accordance with the experiments. Both oscillatory and mean forces are applied simultaneously at initialization.

The mechanical material properties of the membrane at each set of environmental conditions are taken from our previous tensile test measurements in Ref. [17] while the material constants for the SWT model are obtained from the ex-situ fatigue data reported in Ref. [13]. In contrast to experimental fatigue tests where the specimen lifetime is determined only at the most critical position, the current fatigue model is capable of predicting the membrane lifetime distribution across the entire specimen domain. Fig. 2 presents the simulated spatial distribution of the membrane fatigue lifetime under cyclic mechanical loading at room conditions (23 °C, 50% RH) for the maximum stress levels of 22.4 MPa and 18.4 MPa. The membrane lifetime is expressed as the logarithm of the number of load cycles that the membrane can withstand before crack initiation. As expected, the central section of the specimen, shown as area (2) in Fig. 1, withstands fewer cycles than the two rectangular end lobes shown as area (1). This is primarily due to the higher levels of cyclic strains experienced in the narrow central section of the specimen. The overall lifetime-limiting points of the specimen are located at the four corner points of area (2) (e.g., point A in Fig. 1) where the most severe stress and strain fluctuations within this particular geometry are found to occur. The numerical simulation is repeated for the case of fuel cell conditions (70 °C, 90% RH) with results depicted in Fig. 3. In this case, the fatigue lifetime is shorter than at room conditions, although the spatial lifetime distribution appears to be similar. Again, the most critical points of failure are the four corners of the central section (point A). The lifetime at the center point of the domain (point B) is found to be roughly an order of magnitude higher than at point A.

Table 1
Fatigue material constants at four different environmental conditions.

	σ'_f (MPa)	b	ε'_f	c
23 °C, 50% RH	24.50	−0.043	0.9	−0.45
23 °C, 90% RH	16.03	−0.027	0.93	−0.28
70 °C, 50% RH	10.03	−0.032	0.76	−0.22
70 °C, 90% RH	10.6	−0.027	1.13	−0.32

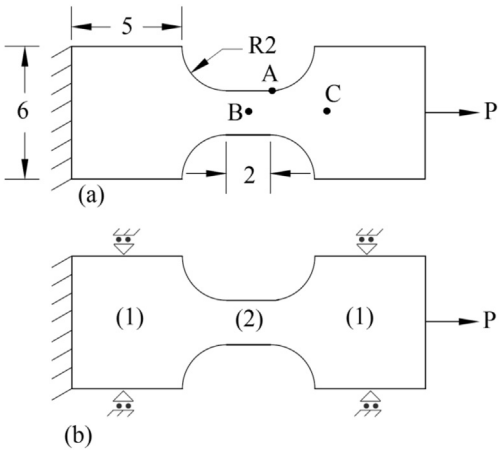

Fig. 1. Dogbone specimen geometry used for the (a) mechanical (b) hygrothermal cyclic simulations, with dimensions given in mm. Positions A, B, and C indicate points of interest in the analysis.

The fatigue model is thoroughly validated by running simulations of all environmental conditions and force levels considered in the previously reported fatigue measurements [13] and comparing the obtained fatigue lifetimes. The selected environmental conditions and applied forces represent a comprehensive set of conditions relevant to fuel cell applications. In all cases, the fatigue model predicts initial fatigue fracture at point A, which was consistently observed in the experiments as well [13], thus verifying the location of the highest stress and strain in the specimen. The simulated fatigue lifetime results at this position are compared against the measured data in Fig. 4. A good agreement is observed between simulated and measured data across the entire range of conditions considered in this work, which verifies the lifetime predictive capabilities of the model. The model is validated with experimental data up to ~10^6 cycles and the simulations are therefore terminated after 10^7 cycles (as indicated by the blue (in web version) regions in Figs. 2–3). Certain deviations are observed at the lower end of the fatigue lifetime spectrum (~10^4 cycles) under high applied stress. As shown experimentally [13], the failures obtained at high mean stress were dominated by material creep as opposed to fatigue. Hence, the fatigue failures predicted by the model were not reached experimentally under these conditions. Overall, the present fatigue model is deemed to be robust and capable of simulating the membrane fatigue lifetime under a wide range of conditions.

Next, the validated model is utilized to examine the strain profile in the membrane during the mechanical fatigue process. The simulated axial strain at points A and B during the first two load cycles are shown in Fig. 5. In this case the specimen is held under fuel cell conditions and subjected to cyclic applied force with a maximum nominal stress of 10.4 MPa. Due to the stress concentration at point A higher strain peaks at the maximum applied stress and deeper valleys at the minimum stress is visible compared to point B. The strain does not recover as much during the force minima, which is a result of plastic deformation. The specific strain pattern observed is dominated by post yield behavior in the initial loading phase followed by more elastic behavior during the unloading phase and subsequent load cycles. The strain recovery during unloading in the second and third quarters of the first cycle is governed by the Young's modulus which is several times larger than the post yield tangent modulus. The nonlinear strain response in the second cycle is also more influenced by the Young's modulus

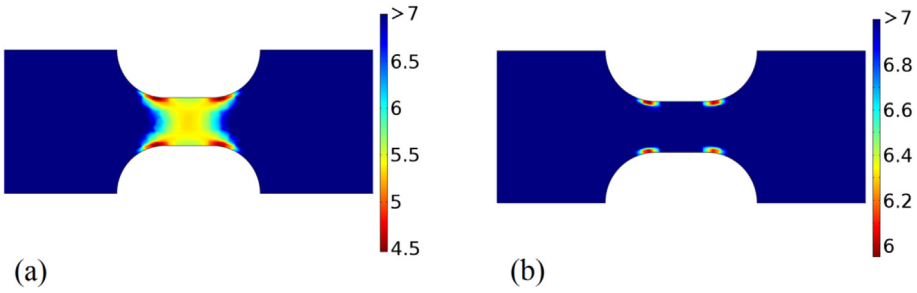

Fig. 2. Simulated membrane fatigue lifetime distribution at room conditions (23 °C, 50% RH) under cyclic mechanical loadings with maximum stress of (a) 22.4 MPa and (b) 18.4 MPa. The lifetime is shown as the logarithm of the number of load cycles at failure.

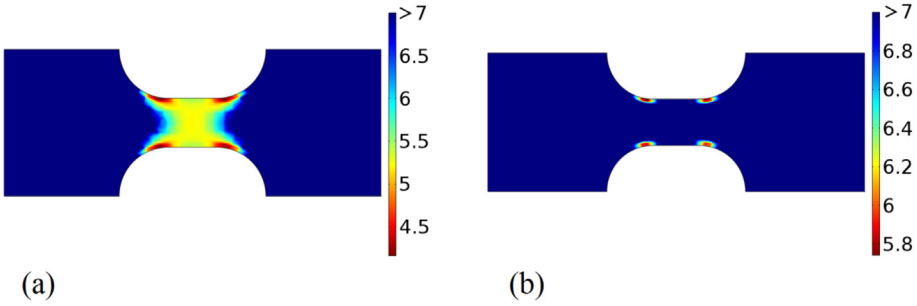

Fig. 3. Simulated membrane fatigue lifetime distribution (logarithmic scale) at fuel cell conditions (70 °C, 90% RH) under cyclic mechanical loadings with maximum stress of (a) 12.8 MPa and (b) 10.4 MPa.

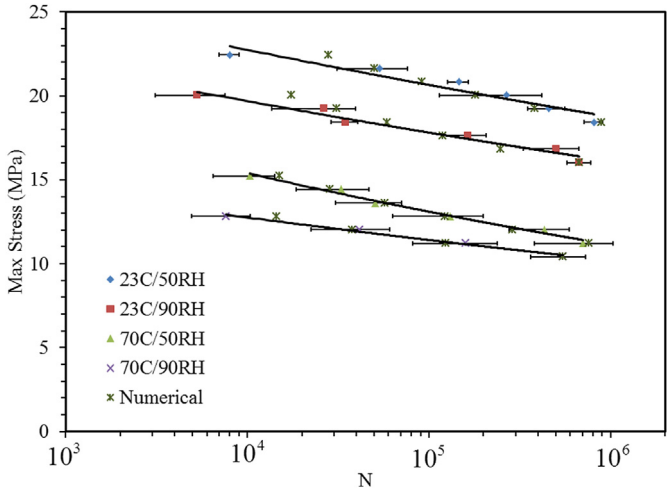

Fig. 4. Comparison of simulated and measured specimen fatigue lifetimes defined by the number of mechanical load cycles at failure (N) at four different sets of environmental conditions [13].

than the post yield tangent modulus. In contrast, the mean value of the oscillating strain is primarily influenced by the post yield tangent modulus rather than the Young's modulus. The strain at point A is consistently higher than at point B due to the stress concentration effect previously mentioned. Although the SWT fatigue model captures both the effects of mean values and amplitudes of the strain oscillations, the shorter fatigue lifetime at point A is attributed to the higher mean strain at this point.

The simulated strain distributions in the membrane specimen are further analyzed in order to seek correlations with the membrane fatigue lifetime distribution previously discussed. The axial strain distributions at the peak applied force after a quarter of the first load cycle are presented in Fig. 6. As expected, the narrow central section of the specimen experiences the highest strain. The maximum levels are found at the edges of the central section (e.g., point A) while the values in the middle of the section (point B) are approximately 25% lower. Although this difference seems small, the 25% reductions in the strain value in this case correspond to two orders of magnitude higher fatigue lifetime than at the edges. This confirms the high sensitivity of the fatigue lifetime to local strains.

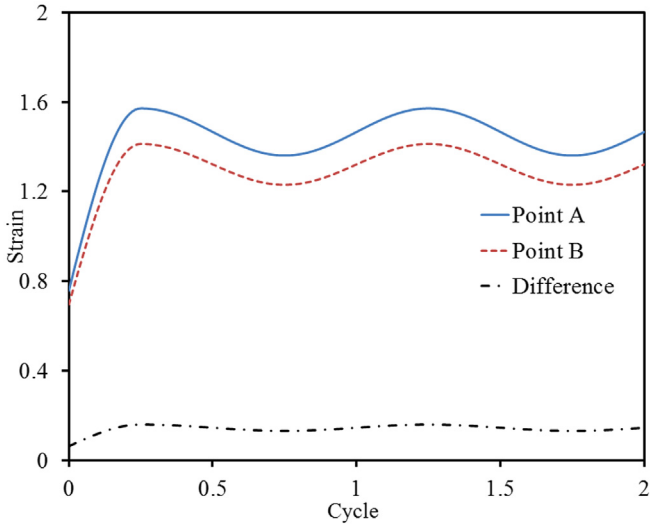

Fig. 5. Variation of strain and at points A and B under cyclic applied force with a maximum stress of 10.4 MPa at fuel cell conditions.

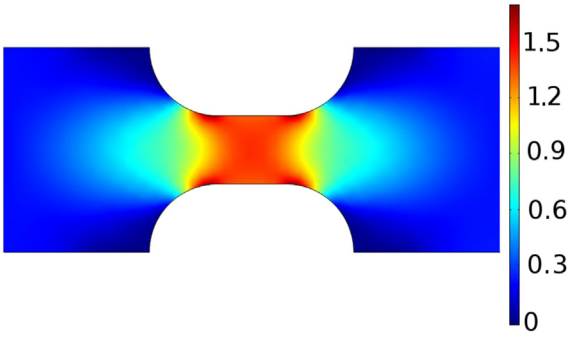

Fig. 6. Strain distributions in the specimen at the peak of the load cycle with a maximum stress of 10.4 MPa at fuel cell conditions.

3.2. Fatigue lifetime simulations under hygrothermal cycles

Having validated the membrane fatigue model under cyclic mechanical loadings for a wide range of environmental conditions, it is now possible to deploy the predictive fatigue lifetime simulations towards stress and strain induced by hygrothermal cycles. Variations in humidity and temperature are known to be the main cause of mechanical membrane degradation during fuel cell operation and further insight into the underlying material fatigue process is desirable. Hence, the validated SWT based fatigue model is applied to study membrane fatigue under specified temperature and humidity cycles. For this purpose, the numerical modeling domain shown in Fig. 1b is devised. In this case, the left edge of the specimen is clamped while the right edge is subjected to a constant time independent distributed load (P). The remaining edges of the specimen are restricted from normal displacement except for the central section which is assigned a free boundary conditions in order to distinguish potential effects of material confinement. The swelling coefficients due to hydration and thermal expansion are adopted from Ref. [44]. Starting from room conditions (23 °C, 50% RH), sinusoidal cycles in either temperature or relative humidity are applied to the specimen. The effect of the initial axial loading is investigated through the nominal engineering stress (σ_n) which is defined here as the average stress in the central section of the specimen.

Fig. 7 shows the simulated fatigue lifetime distributions for two different loading conditions. In the first case, the temperature is cycled between 23 °C and 70 °C at a constant RH of 50% and a nominal stress of 6 MPa. In the second case, the relative humidity is cycled between 50% and 90% at a constant temperature of 23 °C and a nominal stress of 3 MPa. The two different nominal stress levels are chosen in order to reach a comparable fatigue lifetime for each loading condition. Both cases investigated here lead to fatigue fracture after ~10,000 cycles at the same critical point (A) at the edge of the central section as previously observed for mechanical cycling due to local stress/strain concentration. Provided the lower applied nominal stress for humidity cycling, these results indicate that humidity cycling has a stronger effect on the fatigue lifetime than temperature cycling. Temperature cycling is found to be more severe for the central, unconstrained section of the specimen with roughly two orders of magnitude shorter fatigue lifetime than the two rectangular, constrained sections on the periphery. Interestingly, however, humidity cycling results in a much more uniform fatigue lifetime distribution in the specimen.

The simulated strain profiles during temperature and humidity cycling are examined in Fig. 8 at the midpoints of the central (point B) and rectangular end sections (point C) of the specimen. The strain in the material increases with both temperature and humidity and reaches a maximum at the peak conditions. The strain variations during temperature cycling are relatively small and the overall strain is dominated by applied nominal stress, which results in a higher mean strain in the narrow central section (B) than in the wider rectangular end lobes (C). The nominal stress thereby accelerates the fatigue failure during temperature cycling. The humidity cycling conditions, on the other hand, leads to large strain oscillations in both parts of the specimen that substantially outweigh the strain induced by the nominal stress. In this case, the relatively uniform fatigue lifetime distribution correlates to a more uniform strain distribution in the specimen. These findings are supported by the numerical data displayed in Table 2. Overall, the fatigue lifetime is jointly controlled by the amplitude of the strain oscillations and the mean strain induced by the nominal stress in the specimen.

The effect of the mean strain is explored in more detail by varying the nominal stress. As shown in Fig. 9, the fatigue lifetime decreases with increasing nominal stress in all cases. At high amplitudes of strain oscillation, e.g., during large RH swings, the fatigue lifetime is less sensitive to the mean strain value. Hence, the mean strain level is more important during temperature cycling than for RH cycling. Vertical confinement of the membrane appears to have additional effects on the fatigue lifetime. In case of high nominal stress (above the yield point), the fatigue process is more severe in the narrow central section of the specimen (point B) due to higher mean strain in this region. In contrast, when the nominal stress is low, higher strain amplitudes are experienced in the vertically confined regions (point C) and hence lower lifetime is predicted.

The effect of the temperature and relative humidity loading amplitude on membrane fatigue lifetime is demonstrated by the simulated results provided in Fig. 10. For these simulations two different values of nominal stress are considered. The fatigue lifetime is shown to be highly sensitive to the amplitude of the oscillations in all cases. Merely a small reduction in loading amplitude (few %) can result in an order of magnitude increase in lifetime. However, it is also noteworthy that large humidity or temperature amplitudes may lead to “rapid” fatigue failures on the order of 1000

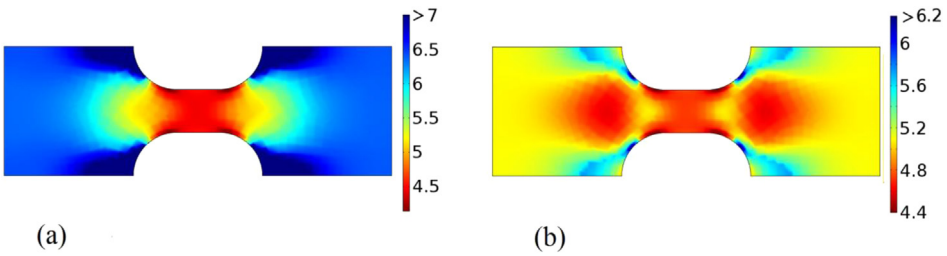

Fig. 7. Simulated membrane fatigue lifetime distribution (logarithmic scale) under (a) temperature cycling between 23 °C and 70 °C at constant relative humidity (50%) and nominal stress (6 MPa) and (b) relative humidity cycling between 50% and 90% at constant temperature (23 °C) and nominal stress (3 MPa).

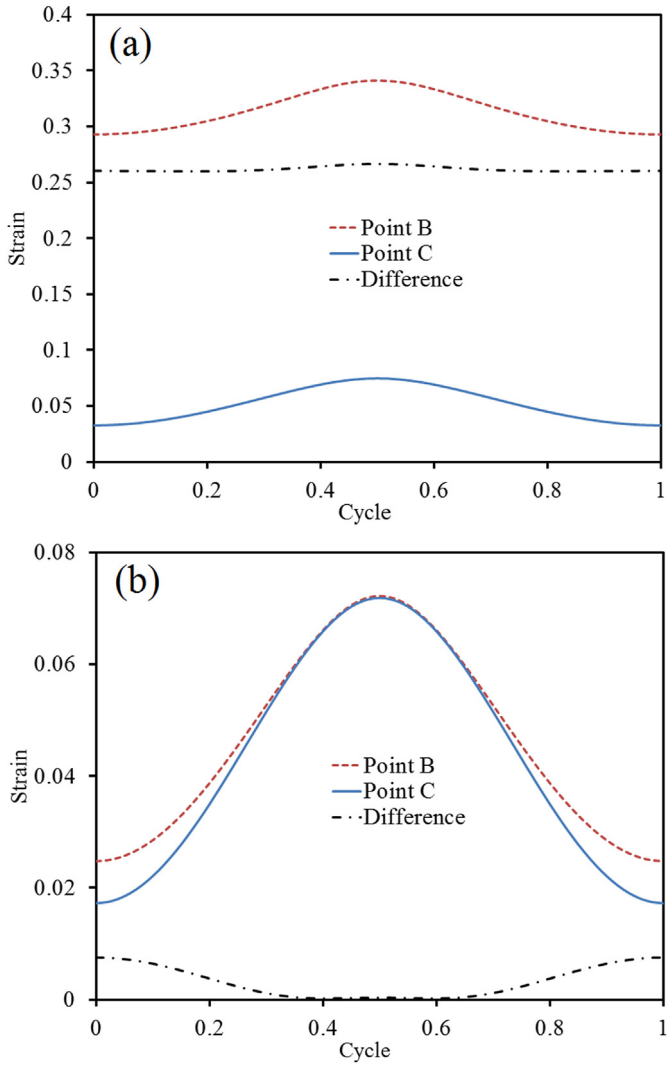

Fig. 8. Simulated strain profiles at points B and C during (a) temperature and (b) humidity cycling.

cycles or less.

So far in the simulations, it has been assumed that only one of the environmental conditions changes while the other one is held constant. In the final step, we assume that both environmental conditions change simultaneously from room conditions (23 °C, 50%) to fuel cell conditions (70 °C, 90%). The simulated results shown in Fig. 11 reveal several interesting trends. A lower nominal stress (0.1 MPa and 2 MPa) is applied here to mitigate the large strain oscillations induced by simultaneous temperature and humidity cycling. The high strain oscillations in this case lead to substantial reductions in fatigue lifetime compared to the previous cases considered in Fig. 7, with failures in less than 1000 cycles

Table 2
Comparison of the amplitude and mean value of the strain oscillations (%) and the corresponding fatigue lifetime (logarithmic) at points B and C during temperature and humidity cycling.

	Point B			Point C		
	Amplitude	Mean	Lifetime	Amplitude	Mean	Lifetime
Temperature	2.4	31.4	4.5	2.1	5.2	5.5
Humidity	2.4	4.7	4.7	2.7	4.3	4.6

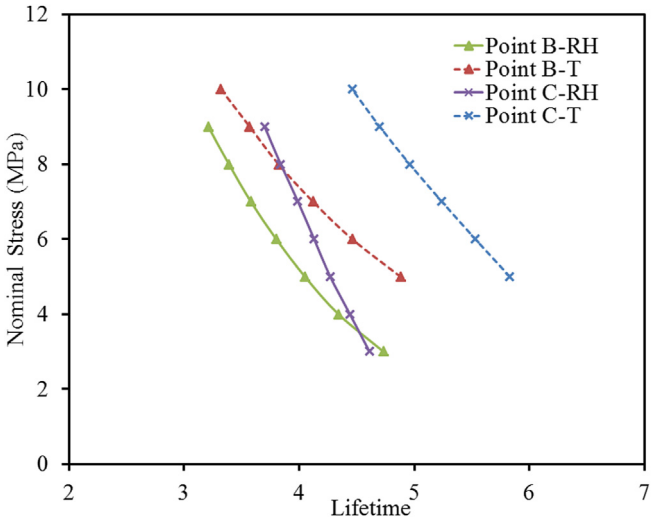

Fig. 9. Simulated membrane fatigue lifetime (logarithmic scale) at points B and C as a function of mean nominal stress for relative humidity and temperature cycling.

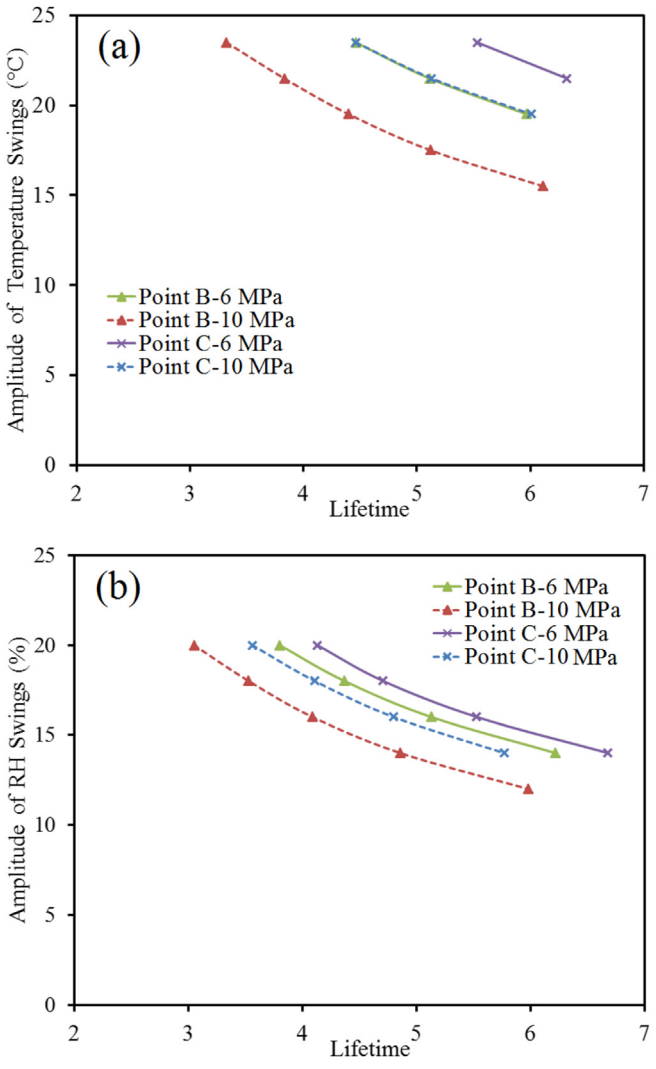

Fig. 10. Simulated membrane fatigue lifetime (logarithmic scale) at points B and C as a function of (a) temperature and (b) relative humidity loading amplitude for two different values of nominal stress (as indicated).

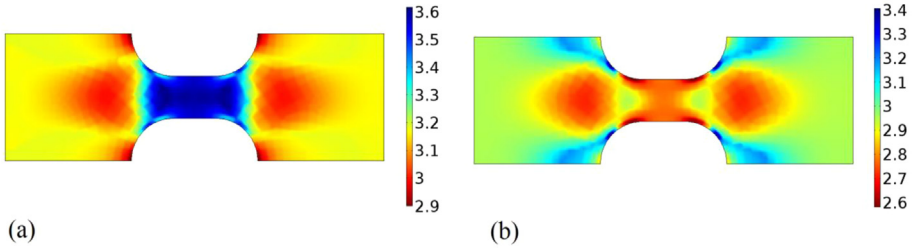

Fig. 11. Simulated membrane fatigue lifetime distribution (logarithmic scale) during hygrothermal cycling between 23 °C, 50% RH and 70 °C, 90% RH under a nominal stress of (a) 0.1 MPa and (b) 2 MPa.

despite the lower applied nominal stress. With low nominal stress (0.1 MPa) the fatigue process is found to be most severe in the rectangular regions around point C, which is attributed to higher local strain amplitude caused by the vertical confinement in these parts. However, as the nominal stress is increased to 2.0 MPa, the mean stress and strain amplitude increase in the middle section as well. Therefore, the fatigue lifetime distribution is more uniform in both parts of the specimen (i.e., points B and C), although the overall lifetime is only marginally shorter due to the shift in failure location to the new stress/strain concentration area at point A. In summary, the fatigue process is shown to be accelerated significantly by combined temperature and humidity variations due to the higher strain amplitudes in effect throughout the specimen domain.

4. Conclusions

An ionomer membrane fatigue model was developed using a customized finite element based Smith-Watson-Topper (SWT) numerical algorithm and utilized to investigate the membrane fatigue behavior under mechanical and hygrothermal cyclic loading conditions. The proposed fatigue model was designed to capture both oscillatory and mean stresses and strains in the specimen. Previously measured experimental data for a dogbone shaped membrane specimen subjected to cyclic mechanical loading at different sets of environmental conditions were used to validate the model. The proposed fatigue model was able to accurately reproduce the membrane fatigue lifetime and failure location under a wide range of applied mechanical loads and environmental conditions from room conditions to fuel cell conditions. When subjected to cyclic mechanical loading, specimen fatigue failure was consistently observed at stress/strain concentration points at the curved edge of the narrow central section of the specimen, in agreement with experimental observations. The fatigue lifetime distribution largely followed the local stress and strain in the specimen.

The validated model was then used to simulate the ex-situ fatigue behaviour of membrane specimens under the application of a constant nominal stress and cyclic hygrothermal loading conditions, which is more relevant for fuel cell operation than mechanical cycling, albeit more challenging and costly to investigate experimentally. The identical position for fatigue failure at the edge of the central section was generally obtained. The simulated fatigue lifetime was significantly shorter under humidity cycling than for temperature cycling due to the higher strain oscillation amplitude. Both the amplitude of the strain oscillations induced by hygrothermal cycling and the mean strain induced by the applied nominal stress had a significant effect on the fatigue lifetime of the specimen. Vertical confinement of the specimen had additionally negative impact on the fatigue lifetime in the case of low nominal stress. The amplitude of the humidity/temperature fluctuations was found to be the most critical parameter, as merely small increases in amplitude led to drastic reductions in lifetime. Furthermore, the simulations predicted that simultaneous cycling of humidity and temperature may induce particularly aggressive fatigue conditions with exacerbated strain amplitudes capable of generating fatigue failures in less than 1000 cycles.

The overall findings of this work demonstrate that ionomer membrane fatigue is important under both mechanical and hygrothermal fluctuations. The present numerical modeling approach is deemed a practical and effective strategy to resolve the spatial variations as well as the coupled effects of constant nominal stress, strain amplitudes during cycling, and specimen confinement on fatigue lifetime. The results and trends identified in this work are expected to be generally valid for membrane fatigue analysis in a wide range of fuel cell applications.

Acknowledgments

Funding for this research provided by Automotive Partnership Canada (APC) and Ballard Power Systems is highly appreciated.

References

[1] Y. Wang, K.S. Chen, J. Mishler, S.C. Cho, X.C. Adroher, Appl. Energy 88 (2011) 981.
[2] N.L. Garland, T.G. Benjaminb, J.P. Kopaszb, ECS Trans. 11 (2007) 923.
[3] J. Wu, X.Z. Yuan, J.J. Martin, H. Wang, J. Zhang, J. Shen, S. Wu, W. Merida, J. Power Sources 184 (2008) 104.
[4] S. Zhang, X. Yuan, H. Wang, W. Merida, H. Zhu, J. Shen, S. Wu, J. Zhang, Int. J. Hydrog. Energy 34 (2009) 388.
[5] N. Macauley, L. Ghassemzadeh, C. Lim, M. Watson, J. Kolodziej, M. Lauritzen, S. Holdcroft, E. Kjeang, ECS Electrochem. Lett. 2 (2013) F33.
[6] L. Gubler, S.M. Dockheer, W.H. Koppenol, J. Electrochem. Soc. 158 (2011) B755.
[7] L. Ghassemzadeh, T.J. Peckham, T. Weissbach, X. Luo, S. Holdcroft, J. Am. Chem. Soc. 135 (2013) 15923.
[8] L. Ghassemzadeh, S. Holdcroft, J. Am. Chem. Soc. 135 (2013) 8181.
[9] K.H. Wong, E. Kjeang, J. Electrochem. Soc. 161 (2014) F823.
[10] C. Lim, L. Ghassemzadeh, F. Van Hove, M. Lauritzen, J. Kolodziej, G.G. Wang, S. Holdcroft, E. Kjeang, J. Power Sources 257 (2014) 102.
[11] R.M.H. Khorasany, M.-A. Goulet, A.S. Alavijeh, E. Kjeang, G.G. Wang, R.K.N.D. Rajapakse, J. Power Sources 252 (2014) 176.
[12] M.N. Silberstein, M.C. Boyce, J. Power Sources 196 (2011) 3452.
[13] R.M.H. Khorasany, A. Sadeghi Alavijeh, E. Kjeang, G.G. Wang, R.K.N.D. Rajapakse, J. Power Sources 274 (2015) 1208.
[14] A. Kusoglu, M.H. Santare, A.M. Karlsson, J. Polym. Sci. Part B Polym. Phys. 49 (2011) 1506.
[15] Y. Tang, A. Kusoglu, A.M. Karlsson, M.H. Santare, S. Cleghorn, W.B. Johnson, J. Power Sources 175 (2008) 817.
[16] X. Huang, R. Solasi, Y.U.E. Zou, M. Feshler, K. Reifsnider, D. Condit, S. Burlatsky, T. Madden, J. Polym. Sci. Part B Polym. Phys. 44 (2006) 2346.
[17] M.A. Goulet, R.M.H. Khorasany, C. De Torres, M. Lauritzen, E. Kjeang, G.G. Wang, N. Rajapakse, J. Power Sources 234 (2013) 38.
[18] M.N. Silberstein, M.C. Boyce, J. Power Sources 195 (2010) 5692.
[19] A. Kusoglu, Y. Tang, M. Lugo, A.M. Karlsson, M.H. Santare, S. Cleghorn, W.B. Johnson, J. Power Sources 195 (2010) 483.
[20] Y. Tang, A.M. Karlsson, M.H. Santare, M. Gilbert, S. Cleghorn, W.B. Johnson, Mater. Sci. Eng. A 425 (2006) 297.
[21] N.S. Khattra, A.M. Karlsson, M.H. Santare, P. Walsh, F.C. Busby, J. Power Sources 214 (2012) 365.
[22] A. Kusoglu, A.M. Karlsson, M.H. Santare, S. Cleghorn, W.B. Johnson, J. Power

Sources 170 (2007) 345.
[23] K.K. Poornesh, Y. Xiao, C. Cho, Fuel Cells 13 (2013) 217.
[24] K. Oh, P. Chippar, H. Ju, Int. J. Hydrog. Energy (2013) 1.
[25] R. Solasi, Y. Zou, X. Huang, K. Reifsnider, Mech. Time-Dependent Mater. 12 (2008) 15.
[26] W. Yoon, X. Huang, J. Power Sources 196 (2011) 3933.
[27] K.K. Poornesh, Y.-J. Sohn, G.-G. Park, T.-H. Yang, Int. J. Hydrog. Energy 37 (2012) 15339.
[28] M.N. Silberstein, P.V. Pillai, M.C. Boyce, Polym. Guildf. 52 (2011) 529.
[29] P.A. García-Salaberri, M. Vera, R. Zaera, Int. J. Hydrog. Energy 36 (2011) 11856.
[30] T. Zarrin-Ghalami, A. Fatemi, Int. J. Fatigue 55 (2013) 92.
[31] Z. Lopez, A. Fatemi, Mater. Sci. Eng. A 556 (2012) 540.
[32] R. Banan, A. Bazylak, J. Zu, Int. J. Hydrog. Energy 38 (2013) 14764.
[33] Y. Kai, J. Fuel Cell. Sci. Technol. 10 (2013) 021007.
[34] Y. Li, J.K. Quincy, S.W. Case, M.W. Ellis, D.A. Dillard, Y.-H. Lai, M.K. Budinski, C.S. Gittleman, J. Power Sources 185 (2008) 374.
[35] E. Moukheiber, C. Bas, L. Flandin, Int. J. Hydrog. Energy 39 (2014) 2717.
[36] R. Solasi, X. Huang, K. Reifsnider, Mech. Mater. 42 (2010) 678.
[37] H. Tang, S. Peikang, S.P. Jiang, F. Wang, M. Pan, J. Power Sources 170 (2007) 85.
[38] T.T. Aindow, J. O'Neill, J. Power Sources 196 (2011) 3851.
[39] A. Sadeghi Alavijeh, M.-A. Goulet, R.M.H. Khorasany, J. Ghataurah, C. Lim, M. Lauritzen, E. Kjeang, G.G. Wang, R.K.N.D. Rajapakse, Decay in mechanical properties of catalyst coated membranes subjected to combined chemical and mechanical membrane degradation, Fuel Cells (2014), http://dx.doi.org/10.1002/fuce.201400040.
[40] Z. Lu, C. Kim, A.M. Karlsson, J.C. Cross, M.H. Santare, J. Power Sources 196 (2011) 4646.
[41] C.D. Lykins, S. Mall, V. Jain, Int. J. Fatigue 22 (2000) 703.
[42] W. Sum, E. Williams, S. Leen, Int. J. Fatigue 27 (2005) 403.
[43] A. Ince, G. Glinka, Fatigue Fract. Eng. Mater. Struct. 34 (2011) 854.
[44] Z. Lu, M. Lugo, M.H. Santare, A.M. Karlsson, F.C. Busby, P. Walsh, J. Power Sources 214 (2012) 130.